Available online at www.sciencedirect.com
ScienceDirect
Earth and Planetary Science Letters 257 (2007) 170–187
EPSL
www.elsevier.com/locate/epsl

A new noble gas paleoclimate record in Texas — Basic assumptions revisited

Maria Clara Castro [a,*], Chris Michael Hall [a], Delphine Patriarche [b,1], Patrick Goblet [c], Brian Robert Ellis [a,2]

[a] University of Michigan, Department of Geological Sciences, 2534 C. C. Little Building, Ann Arbor, MI 48109 - 1005, United States
[b] Commissariat à l'Energie Atomique, 91680 Bruyères-le-Châtel, France
[c] Ecole des Mines de Paris, Centre de Géosciences, 77305 Fontainebleau, France

Received 25 July 2006; received in revised form 19 February 2007; accepted 19 February 2007
Available online 27 February 2007
Editor: R.D. van der Hilst

Abstract

A generally accepted basic principle in relation to the use of the noble gas thermometer in groundwater flow systems is that high-frequency noble gas climatic signals are lost due to the effect of dispersion. This loss of signal, combined with ^{14}C dating issues, makes it only suited to identify major climatic events such as the Last Glacial Maximum (LGM). Consequently, the identification of significant noble gas temperature (NGT) cooling (≥ 5 °C) with respect to present time has systematically been associated with the occurrence of the LGM even when reasonable water age controls were unavailable. It has also become apparent at a number of studied sites that modern NGTs estimated through standard models [M. Stute, P. Schlosser, Principles and applications of the noble gas paleothermometer, in: P.K. Swart, K.C. Lohmann, J.A. McKenzie, S. Savin, (Eds), Climate change in continental isotopic records, Geophysical monograph 78, AGU (1993) 89-100.; W. Aeschbach-Hertig, F. Peeters, U. Beyerle, R. Kipfer, Paleotemperature reconstruction from noble gases in ground water taking into account equilibration with entrapped air, Nature 405(6790) (2000) 1040-1044.] are unable to reproduce ground temperatures at the interface with the unsaturated zone, a basic requirement for proper paleoclimate reconstruction through noble gases. Instead, a systematic bias to low NGTs in recharge areas is observed. The Carrizo aquifer, in which the LGM was previously identified [M. Stute, P. Schlosser, J.F. Clark, W.S. Broecker, Paleotemperatures in the Southwestern United States derived from noble gases in ground water, Science 256(5059) (1992) 1000-1001.] and which presents an NGT bias of over 4 °C, is an ideal setting to analyze and revise basic principles and assumptions in relation with the use of the noble gas thermometer.

Here, we present a new noble gas data set (49 measurements) collected at 20 different locations in the Carrizo aquifer. This new data set together with previously published data (20 measurements) was used to calibrate a 3-D groundwater flow and ^{4}He transport model in which simulations of groundwater age were subsequently carried out. These account for mixing processes due to advection, dispersion, diffusion, and cross-formational flow.

We first show that samples previously attributed to the LGM belong in fact to the middle Holocene. Through a step-by-step approach we then proceed to carry out a comparative analysis of both the impact of dispersion on high frequency climatic signals and assumptions underlying competing NGT models. Our combined analysis indicates that groundwater flow systems, at least

* Corresponding author. Tel.: +1 734 615 3812; fax: +1 734 763 4690.
E-mail addresses: mccastro@umich.edu (M.C. Castro), cmhall@umich.edu (C.M. Hall), delphine.patriarche@gazdefrance.com (D. Patriarche), patrick.goblet@ensmp.fr (P. Goblet), brellis@Princeton.EDU (B.R. Ellis).
[1] Now at Gaz de France, 361, avenue du President Wilson, 93211 La Plaine Saint Denis, France.
[2] Now at Princeton University, Department of Civil and Environmental Engineering, E-223 E-Quad, Princeton, NJ 08540.

doi:10.1016/j.epsl.2007.02.030

those with similar characteristics to that of the Carrizo, do have the ability to preserve short term (100–200 yrs) climatic fluctuations archived by noble gases. It also shows that abrupt climate shifts during the mid-late Holocene which are associated with significant NGT changes (≥5 °C) do not reflect equally important changes in the mean annual atmospheric temperature (MAAT). Instead, these reflect the combined effect of atmospheric temperature changes, seasonality of recharge and, above all, significant variations of the water table depth which result from shifts between humid and arid regimes. Together with NGTs, our excess air record plays a critical role in identifying such abrupt climate changes. Specifically, the Carrizo combined data set indicates an abrupt shift from a cool, humid regime to a warmer, arid one at ~ 1 kyrs BP. A major Holocene (~ 6 kyrs BP) NGT change of 7.7 °C with respect to present now identified is mostly the result of a dramatic water table drop which occurred during the ~ 1 kyrs BP transition period. Current NGTs in the Carrizo recharge area do not appear to be recording atmospheric changes. Rather, these are recording ground conditions reflecting mostly the impact of heat flow in the area. We also show that observed systematic offsets in NGT recharge areas can be reconciled through NGT estimation models which account for a noble gas partial pressure increase in the unsaturated zone, potentially due to O_2 depletion.

Keywords: noble gas temperatures; groundwater flow modeling; simulation of groundwater ages; high-frequency climatic signals; dispersion

1. Introduction

Because noble gases (Ne, Ar, Kr, and Xe) are conservative tracers and their concentrations in the recharge areas of groundwater systems are typically considered to be simply a function of temperature, altitude, excess air, and salinity, noble gas temperatures (NGTs) are commonly regarded as a potentially robust indicator of past climate [1–3].

Meaningful paleoclimatic reconstructions through NGTs, however, require a number of conditions and basic assumptions to be fulfilled (e.g., [4]). The most immediate one is availability of reasonably accurate water age information. Correspondence between NGTs and groundwater age has been typically done based on ^{14}C ages, a dating tool that remains problematic in many groundwater flow systems (e.g., [5–7]). Another generally accepted basic principle is that high-frequency noble gas climatic signals are lost or severely diminished in most groundwater systems due to the effect of dispersion [1,2]. Because of the combined effect of high-frequency signal loss and ^{14}C dating issues, it was concluded that the noble gas thermometer cannot be used to identify short-term climatic fluctuations, but instead, is only suited to identify major climatic events such as the Last Glacial Maximum (LGM) [3]. Consequently, the identification of important cooling (≥5 °C) with respect to present time through NGTs has systematically been associated with the occurrence of the LGM. In some cases, such associations have been made despite the lack of reasonable water age controls (e.g., [8,5]).

Another basic requirement for the application of the noble gas thermometer is that noble gases should closely record the mean annual temperature at the water table, i.e., the ground temperature at the interface with the saturated zone [3,1]. Until recently, with the exception of estimated water table NGTs systematically lower (~ 2.2 °C) with respect to soil temperature observed in Bocholt, Germany [4], no other NGT biases in recharge areas have been reported in the literature. Such depressed NGTs were attributed to the effect of vegetation, presumably due to depressed ground temperature. A recent and detailed study in southern Michigan [9,10], however, also found that estimated water table NGTs were systematically depressed with respect to ground temperature. These were estimated using the two most common and widely accepted models, i.e., the unfractionated air (UA) model as developed by Stute and Schlosser [1], and the continuous equilibration (CE) model [11]. As demonstrated by Hall et al. [10], both models display differing (2.5–4 °C) but systematically depressed NGTs compared to ground temperature at the interface with the water table. A closer look at previously published NGT data indicates that at least in some cases, equally important biases are observed elsewhere. For example, temperature measurements in recharge waters of the Carrizo aquifer, southwestern Texas (e.g., [12]) indicate that previously reported [8,13] NGTs in this area are also depressed with respect to ground temperature by ~ 4.2 °C. This significant bias to low NGTs in recharge areas in very distinct climatic regions, i.e., temperate (Germany, southeastern Michigan) versus semi-arid (southwest Texas) is a clear indication that assumptions of both the UA and CE models do not adequately describe all the mechanisms controlling noble gas concentrations (e.g., increased noble gas partial pressure, modification of gas solubility due to reduced soil humidity, etc.) and thus, NGTs in these areas (e.g., [14,10]).

Issues of groundwater dating and preservation or loss of high versus low frequency climatic signals in groundwater systems are intrinsically related to the specific characteristics of each individual system. As already pointed out by

Favreau et al. [15], in order to correctly interpret NGT records as well as to improve our understanding of the mechanisms controlling the original input of atmospheric noble gas concentrations, a reasonable knowledge of the dynamics of the groundwater system in question both in the confined and unconfined areas is required. Improved and increased density data sets will also play a critical role in reaching such goals.

Groundwater flow, heat transfer, and helium transport in the Carrizo aquifer and surrounding formations have been extensively studied in recent years (e.g., [12,16–18]). Such studies were carried out with the aide of 1-, 2-, and 3-D numerical and geostatistical models through incorporation of large primary data sets. Issues of groundwater age estimation in this particular system have also been analyzed [7]. This background work together with a new noble gas data set renders the Carrizo aquifer an ideal candidate to further analyze and deepen our understanding of the information archived by the noble gas thermometer in groundwater flow systems.

Here, through a combination of 3-D simulations of groundwater flow, ^{4}He transport, and groundwater ages as well as a comparative analysis of both the impact of dispersion on high-frequency climatic signals and assumptions underlying competing NGT models, we address some basic issues in relation to the use of the noble gas thermometer in groundwater flow systems. Our analysis is based on the combined previously published [8,19] and new (this study) data sets.

Overall this work attempts to clarify a number of issues relating to the use of the noble gas thermometer in groundwater flow systems and to address apparent inconsistencies between NGTs and ground temperature which, at present, widely used and sophisticated NGTs models (e.g., UA, CE) remain unable to resolve.

2. Geological and hydrogeological background

The Carrizo aquifer, a major groundwater flow system in Texas, is part of a thick regressive sequence of terrigenous clastics that formed within fluvial, deltaic and marine depositional systems in the Rio Grande Embayment area of South Texas on the northwestern margin of the Gulf Coast Basin (Fig. 1a).

In the study area (Fig. 1b) the Carrizo aquifer is a confined, massive sandstone lying unconformably on the Wilcox formation (Fig. 1c; [20,21]). Downdip, the Carrizo contains an increasing amount of shales and mudstones [22,23]. The thickness of the Carrizo is highly variable, ranging from 50 m in the southern part of McMullen County to about 350 m in the northern part of Live Oak County. The underlying lower-Wilcox, the oldest formation of Tertiary age, contains thick mudstone and clay layers. The Recklaw formation, a confining layer primarily composed of shale, fine sand and marine mudstones, conformably overlies the Carrizo aquifer and is in turn overlain by the Queen City aquifer that consists of thick coastal barrier sands in the study area. These formations outcrop subparallel to the present-day coastline as a southwest–northeast wide band across Texas. Dip is to the southeast (Fig. 1a, c). The Carrizo aquifer terminates at a major 32 km wide growth–fault system commonly known as the Wilcox Geothermal Corridor (Fig. 1a, b). Groundwater flows gravitationally from the outcrop areas toward the southeast. Discharge occurs by cross-formational upward leakage along the entire formation, and along fault-related permeability pathways.

3. Sample collection and measurements

Groundwater samples were collected from 20 wells in the Carrizo aquifer (Fig. 1, Table 1) for measurement of noble gases (Table 2). Replicates were collected at multiple locations resulting in a total of 49 analyzed samples. Water samples were collected in 3/8″ Cu tubes clamped at both ends and analyzed for He, Ne, Ar, Kr and Xe using an automated noble gas extraction system connected to a MAP215 mass spectrometer. Noble gases were analyzed at the University of Michigan. Sampling and measurement procedures are reported elsewhere [9,24]. Ne, Ar, Kr and Xe isotope ratios are identical to air within measurement precision.

Among the 20 wells now sampled, only one (CTX03, Table 1) corresponds to one of the 22 set of previously sampled wells (TX03 [8,19]). With this new sampling collection noble gas analyses are now available at 41 different locations in the study area (Fig. 1b).

4. ^{4}He systematics and results

^{4}He measurements from this new sampling campaign together with previously published data [19] were used to recalibrate a 3-D groundwater flow and ^{4}He transport model ([17], Fig. 1b), prior to simulation of groundwater ages (Section 5).

^{4}He concentrations ($^4He_{meas}$) in groundwater frequently exceed those expected for water in solubility equilibrium with the atmosphere (Air Saturated Water: ASW; $^4He_{eq}$). Observed ^{4}He excesses in groundwater ($^4He_{exc}$) have either a mantle or crustal (radiogenic) origin. The latter results from α decay of the natural U and Th decay series present in many common rocks. In groundwater systems, these excesses can result either from in-situ production (production taking place within the groundwater flow system in

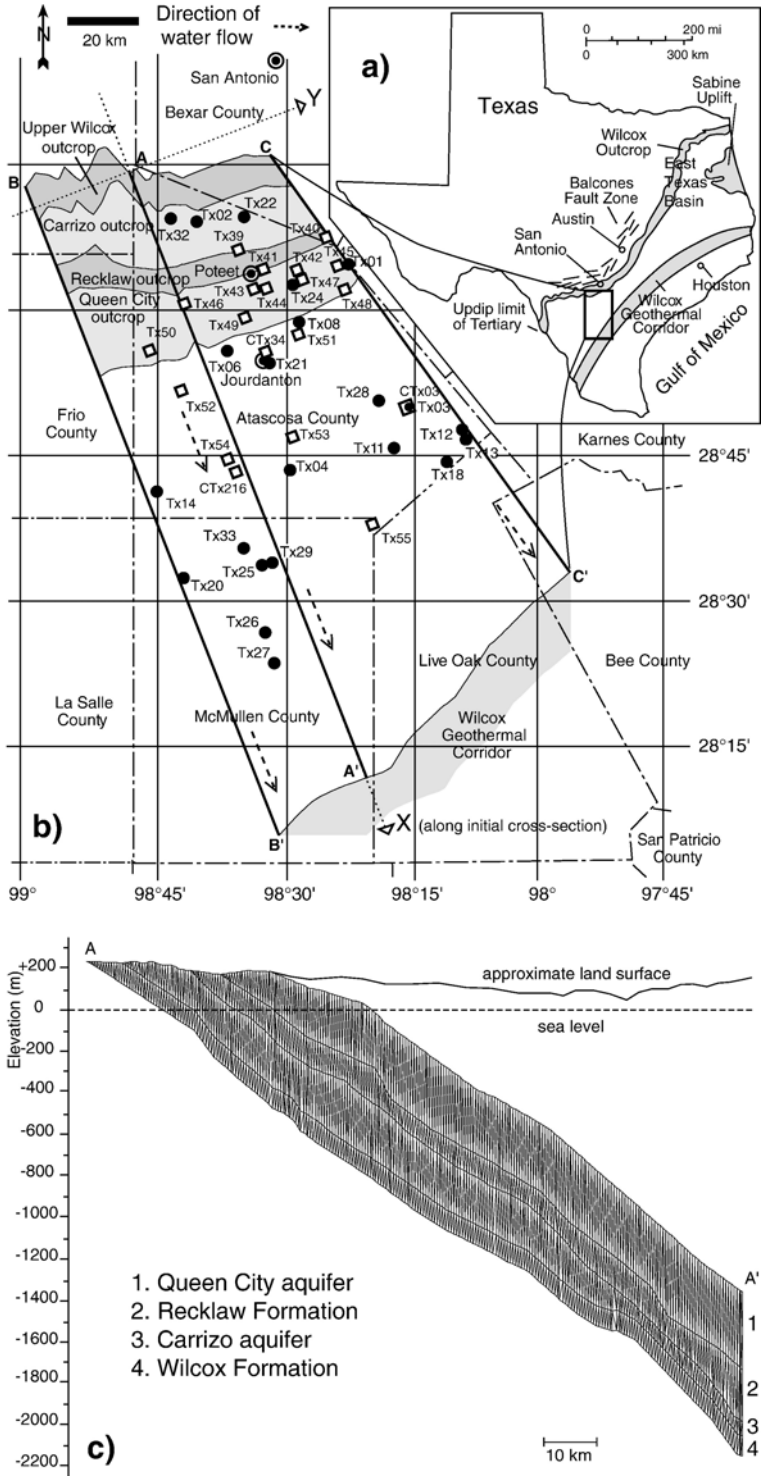

Fig. 1. a) Location and tectonic setting of the study area in Texas after Hamlin [21]. b) Detailed representation of the study area and delineation of the region covered by the 3-D model. Lateral boundaries of the 3-D model (BB′ and CC′) as well as cross-section AA′ [15] shown as bold black lines; locations of previously published [8,19] and new (this study) noble gas samples shown as closed circles and open squares, respectively; c) simplified representation of cross-section along AA′.

Table 1
Well identification and location for new samples (this study) collected in the study area

Well name	Well number	Latitude	Longitude	Distance [a]	Bottom well elevation ASL [b]
				(km)	(m)
Tx39	6860119	29.09948	−98.60350	9.91	26.5
Tx40	6861203	29.12218	−98.43765	11.51	37.8
Tx41	6860530	29.06772	−98.55563	15.03	−89.9
Tx42	6861413	29.06732	−98.49215	17.39	−216.0
Tx43	6860850	29.03444	−98.57361	17.73	−193.5
Tx44	6860852	29.03560	−98.54985	18.55	−222.5
Tx45	6861205	29.07525	−98.41560	17.79	−162.2
Tx46	6859804	29.00833	−98.70361	20.00	−74.4
Tx47	6861401	29.05111	−98.48167	19.50	−156.7
Tx48	6861905	29.03528	−98.40167	23.10	−283.8
Tx49	7804107	28.98653	−98.58942	24.85	−216.7
Tx50	78026– –	28.92968	−98.76865	27.86	−322.8
Tx51	7805124	28.96000	−98.48833	28.73	−403.9
CTx34	7804820	28.93000	−98.54944	32.13	−457.2
Tx52	7811217	28.86333	−98.70806	39.19	−408.1
Tx53	7813704	28.78861	−98.49694	48.77	−752.9
Tx54	78127– –	28.75005	−98.61888	55.57	−668.7
CTx216	7820101	28.72889	−98.60306	56.63	−710.2
CTx03	7814302	28.84081	−98.28168	48.87	−901.7
Tx55	7822702	28.64483	−98.34508	66.61	−1194.2

[a] From origin of Carrizo outcrop in the 3-D model.
[b] Above Sea Level.

question) or have an external origin, from deeper layers or from the crystalline basement (e.g., [25–27]). In the latter case, ^{4}He must be transported to the upper levels either through advection, dispersion and diffusion or a combination of these transport processes [27]. In recharge waters a non-negligible excess air component ($^4He_{ea}$) resulting from dissolution of small air bubbles during fluctuations of the water table [28] might be present. $^4He_{eq}$ and $^4He_{ea}$ are estimated based on recharge temperatures (Table 2) derived from Ne, Ar, Kr, and Xe concentrations [29], and $^4He_{exc} = {}^4He_{meas} - {}^4He_{eq} - {}^4He_{ea}$. The 3-D ^{4}He transport model was calibrated with respect to ^{4}He measured concentrations for which the excess air component has been subtracted ($^4He_{noea}$), i.e., with respect to $^4He_{noea} = {}^4He_{meas} - {}^4H_{ea}$ ([19,30], Table 2, this study).

While previous work in the Carrizo aquifer ([19]; Fig. 1b) show excesses of ^{4}He up to two orders of magnitude, $^4He_{exc}$ in our new samples reach a maximum of ~ 45 times that of ASW (Table 2). These excesses, which increase with recharge distance from the outcrop as well as with depth, reflect the incorporation of in-situ and external (crustal and/or mantle) ^{4}He that is progressively added to recharge water entering with an atmospheric ^{4}He component. Smaller ^{4}He excesses of our new data set reflect the closer proximity to the recharge area and shallower depths of the sampled wells which, in turn, translate into younger water ages (Section 5).

5. 3-D conceptual model and calibration results — groundwater flow, ^{4}He transport, and groundwater ages

Coupled groundwater flow and ^{4}He transport simulations as well as direct simulation of groundwater ages were carried out in a 3-D model encompassing four stratigraphic units, the Carrizo and overlying Queen City aquifers, and the Recklaw and upper-Wilcox confining layers (Fig. 1b, c). The 3-D model [17], which comprises 5,089,848 elements and covers a surface of ~ 7000 km^2 (Fig. 1b) represents the exact topography of the different formations both at the surface and at depth. Further information on the 3-D model can be found elsewhere [17]. Mathematical formulation and numerical approach, as well as boundary conditions, calibration data and parameter values can be found in Appendix A.

Prior work on the 3-D model [17] has shown that groundwater flow and ^{4}He concentrations are best described by an exponential decrease of hydraulic conductivities as a function of depth (see also, e.g., [35]). Here, we present the results of a new calibration of the 3-D groundwater flow and transport models which take advantage of additional information obtained from recent heat flow simulations in the area [12], as well as a much richer ^{4}He data set now available.

Exponential decreases of hydraulic conductivity with depth obtained through calibration of the 3-D model with 149 measured hydraulic heads [17] in the Wilcox (K_w), Carrizo (K_c), Recklaw (K_r) and Queen City (K_q) formations are as follow:

$$\begin{aligned} K_w &= 1.09^{*}10^{-11}\exp((z-z_w)/3985) \\ K_c &= 3.5^{*}10^{-4}\exp((z-z_c)/252) \\ K_r &= 1.7^{*}10^{-8}\exp((z-z_r)/252) \\ K_q &= 2.94^{*}10^{-4}\exp((z-z_q)/310) \end{aligned} \quad (4)$$

where z is the altitude at the center of the element at a location of interest, and z_w, z_c, z_r, and z_q are the altitudes at the center of the element located on the outcrops of the Wilcox, Carrizo, Recklaw, and Queen City, respectively. Calculated and measured hydraulic heads, which decrease from the outcrops toward the discharge area are extremely well correlated (r^2=0.98; Fig. 2a, b).

Calibration of the ^{4}He transport model based on a total of 71 measurements (cf., Section 3; Fig. 2c, d) was achieved by prescribing a flux entering the base of the Carrizo of $1^{*}10^{-15}$ mol m^{-2} s^{-1}. Note that, as previously discussed [12], this flux is not representative of the crustal ^{4}He flux. Rather, it reflects the impact of

Table 2
Noble gas concentrations, He component concentrations and unfractionated air (UA) model NGT values

Sample	He_{meas}	$^4He_{noea}$ [a] ($\pm1\sigma$)	$^4He_{exc}$ [a] ($\pm1\sigma$)	Ne	Ar	Kr	Xe	UA_NGT [b] ($\pm1\sigma$)	Excess air ($\pm1\sigma$)	χ^2	3-D model age
	(10^{-8} cm^3 STP g^{-1})	(10^{-8} cm^3 STP g^{-1})	(10^{-9} cm^3 STP g^{-1})	(10^{-7} cm^3 STP g^{-1})	(10^{-4} cm^3 STP g^{-1})	(10^{-8} cm^3 STP g^{-1})	(10^{-9} cm^3 STP g^{-1})	(°C)	(10^{-3} cm^3 STP g^{-1})		(yr)
TX39.1	7.377	5.25(0.34)	8.63(1.11)	2.528	3.614	7.540	9.300	19.05(1.44)	4.06(0.61)	20.41	98.1
TX39.2	7.479	5.06(0.18)	6.80(1.12)	2.642	3.596	7.486	9.767	19.08(0.60)	4.61(0.26)	3.45	”
TX40.1	8.159	6.58(0.16)	21.20(1.22)	2.445	3.683	8.216	11.562	14.34(0.41)	3.02(0.19)	0.47	215.8
TX40.2	10.341	8.49(0.19)	40.16(1.55)	2.544	3.862	8.505	11.649	13.36(0.40)	3.54(0.19)	1.19	”
TX41.1	7.539	5.46(0.28)	10.65(1.13)	2.531	3.619	7.708	9.625	18.18(1.15)	3.97(0.50)	13.46	406.2
TX41.2	7.591	5.58(0.24)	11.85(1.14)	2.507	3.592	7.588	9.678	18.39(0.95)	3.84(0.41)	9.26	”
TX41.3	8.087	6.09(0.23)	16.88(1.21)	2.510	3.590	7.652	9.756	18.16(0.88)	3.82(0.38)	7.97	”
TX42.1	27.315	25.17(0.43)	207.0(4.1)	2.644	3.855	8.270	11.961	13.96(0.53)	4.10(0.26)	3.32	685.3
TX43.1	8.327	6.80(0.20)	24.42(1.25)	2.313	3.324	7.123	9.050	20.64(0.74)	2.91(0.29)	5.36	868.1
TX43.2	8.387	6.96(0.18)	25.70(1.26)	2.309	3.442	7.371	9.710	18.61(0.58)	2.72(0.23)	3.55	”
TX43.3	8.758	7.23(0.26)	28.44(1.31)	2.329	3.486	7.303	9.429	19.06(1.04)	2.92(0.42)	11.16	”
TX44.1	9.637	8.15(0.23)	37.74(1.45)	2.308	3.398	7.191	9.230	19.87(0.87)	2.85(0.34)	7.54	891.0
TX44.2	11.176	8.78(0.20)	44.01(1.68)	2.644	3.502	7.525	9.740	19.41(0.46)	4.57(0.20)	1.23	”
TX44.3	9.480	8.34(0.17)	39.73(1.42)	2.195	3.249	7.139	9.241	20.12(0.49)	2.17(0.19)	2.48	”
TX45.1	8.567	6.72(0.21)	23.37(1.29)	2.440	3.484	7.332	9.471	19.42(0.77)	3.53(0.31)	5.81	889.6
TX45.2	8.789	6.86(0.22)	24.61(1.32)	2.492	3.571	7.724	9.868	17.84(0.77)	3.68(0.33)	6.23	”
TX46.1	9.683	7.98(0.18)	35.47(1.45)	2.461	3.609	8.017	10.866	15.78(0.42)	3.25(0.19)	0.35	959.7
TX46.2	8.445	7.87(0.17)	34.57(1.27)	2.031	3.341	7.323	9.789	17.86(0.57)	1.12(0.21)	3.75	”
TX46.3	9.183	8.23(0.17)	38.24(1.38)	2.167	3.418	7.534	10.011	17.36(0.48)	1.82(0.19)	2.64	”
TX47.1	11.033	9.85(0.19)	54.25(1.65)	2.265	3.495	7.744	10.431	16.51(0.42)	2.26(0.17)	0.86	886.4
TX47.2	10.706	9.71(0.24)	52.82(1.61)	2.193	3.545	7.764	10.169	16.28(0.85)	1.91(0.35)	8.52	”
TX47.3	10.775	9.63(0.19)	52.24(1.62)	2.233	3.476	7.546	10.147	17.22(0.47)	2.18(0.19)	2.52	”
TX48.1	8.920	7.67(0.18)	32.50(1.34)	2.281	3.483	7.749	10.171	16.91(0.52)	2.40(0.21)	3.04	1566.0
TX48.2	8.590	7.49(0.16)	31.05(1.29)	2.202	3.282	7.127	9.903	19.23(0.44)	2.11(0.17)	0.85	”
TX48.3	8.684	7.63(0.16)	32.30(1.30)	2.192	3.402	7.419	9.853	17.99(0.49)	2.01(0.19)	2.62	”
TX49.1	7.104	6.50(0.13)	21.47(1.07)	1.998	3.046	6.675	9.134	21.55(0.45)	1.16(0.15)	0.52	1832.7
TX49.2	8.581	7.42(0.16)	30.08(1.29)	2.253	3.433	7.616	10.441	17.00(0.42)	2.21(0.17)	0.03	”
TX49.3	8.433	7.45(0.20)	30.56(1.26)	2.157	3.382	7.341	9.551	18.48(0.77)	1.88(0.30)	6.47	”
TX50.1	9.077	8.38(0.20)	39.40(1.36)	2.105	3.544	7.810	10.520	15.44(0.67)	1.34(0.27)	5.66	3742.7
TX50.2	9.034	7.99(0.20)	35.90(1.36)	2.188	3.438	7.506	9.798	17.69(0.73)	1.99(0.29)	6.02	”
TX50.3	9.187	8.28(0.16)	38.38(1.38)	2.189	3.508	7.835	10.894	15.49(0.41)	1.74(0.17)	0.06	”
TX51.1	9.091	8.17(0.16)	37.45(1.36)	2.172	3.461	7.665	10.339	16.55(0.41)	1.77(0.17)	1.47	3078.6
TX51.2	9.265	8.27(0.18)	38.45(1.39)	2.205	3.496	7.572	10.887	16.21(0.51)	1.90(0.21)	3.05	”
TX51.3	9.057	8.07(0.16)	36.41(1.36)	2.206	3.469	7.769	10.628	16.12(0.41)	1.89(0.17)	0.17	”
CTX34.1	9.008	8.04(0.16)	36.03(1.35)	2.212	3.515	7.823	11.097	15.38(0.41)	1.84(0.17)	0.60	4319.4
CTX34.2	9.498	8.50(0.17)	40.55(1.42)	2.230	3.550	8.026	11.127	14.85(0.40)	1.90(0.17)	0.11	”
TX52.1	13.864	13.00(0.28)	85.18(2.08)	2.206	3.803	8.524	11.413	12.57(0.83)	1.64(0.36)	9.35	6482.1
TX52.2	15.264	14.30(0.25)	98.11(2.29)	2.253	3.743	8.464	11.827	12.68(0.39)	1.85(0.17)	0.52	”
TX52.3	13.798	13.03(0.22)	85.95(2.07)	2.136	3.464	7.763	10.786	15.72(0.41)	1.47(0.16)	0.03	”
TX53.1	30.502	29.99(0.47)	255.4(4.6)	2.065	3.517	8.144	10.878	14.36(0.54)	0.97(0.22)	3.86	21216.8
TX53.2	29.900	29.37(0.46)	249.2(4.5)	2.072	3.540	8.111	11.013	14.23(0.39)	1.00(0.16)	1.99	”
TX54.1	46.234	45.67(0.74)	412.8(6.9)	1.999	3.301	7.274	9.014	19.01(1.35)	1.08(0.49)	20.50	25586.2
CTX216.1	46.960	46.59(0.71)	421.6(7.0)	1.995	3.365	7.816	10.373	15.89(0.56)	0.71(0.21)	3.85	30840.7
CTX216.2	48.574	48.08(0.74)	436.5(7.3)	2.036	3.410	7.813	10.382	15.85(0.52)	0.95(0.20)	3.37	”
CTX03.1	123.608	122.1(1.9)	1176(19)	2.401	3.683	8.245	10.852	14.81(0.59)	2.88(0.26)	4.17	47544.8
CTX03.2	98.002	97.62(1.47)	932.0(14.7)	1.989	3.317	7.673	10.151	16.60(0.55)	0.74(0.21)	3.69	”
TX55.1	194.517	192.8(2.9)	1884(29)	2.392	3.415	7.264	9.196	20.04(0.86)	3.31(0.35)	7.26	246444.6
TX55.2	194.372	192.6(2.9)	1882(29)	2.445	3.658	7.906	10.186	16.52(0.89)	3.33(0.39)	8.88	”
TX55.3	201.381	199.6(3.0)	1952(30)	2.453	3.633	7.911	10.207	16.61(0.78)	3.36(0.34)	6.72	”
Error (1σ)	1.5%			1.3%	1.3%	1.5%	2.2%				

[a] Calculated using the UA model.
[b] Average recharge altitude is 200 m.

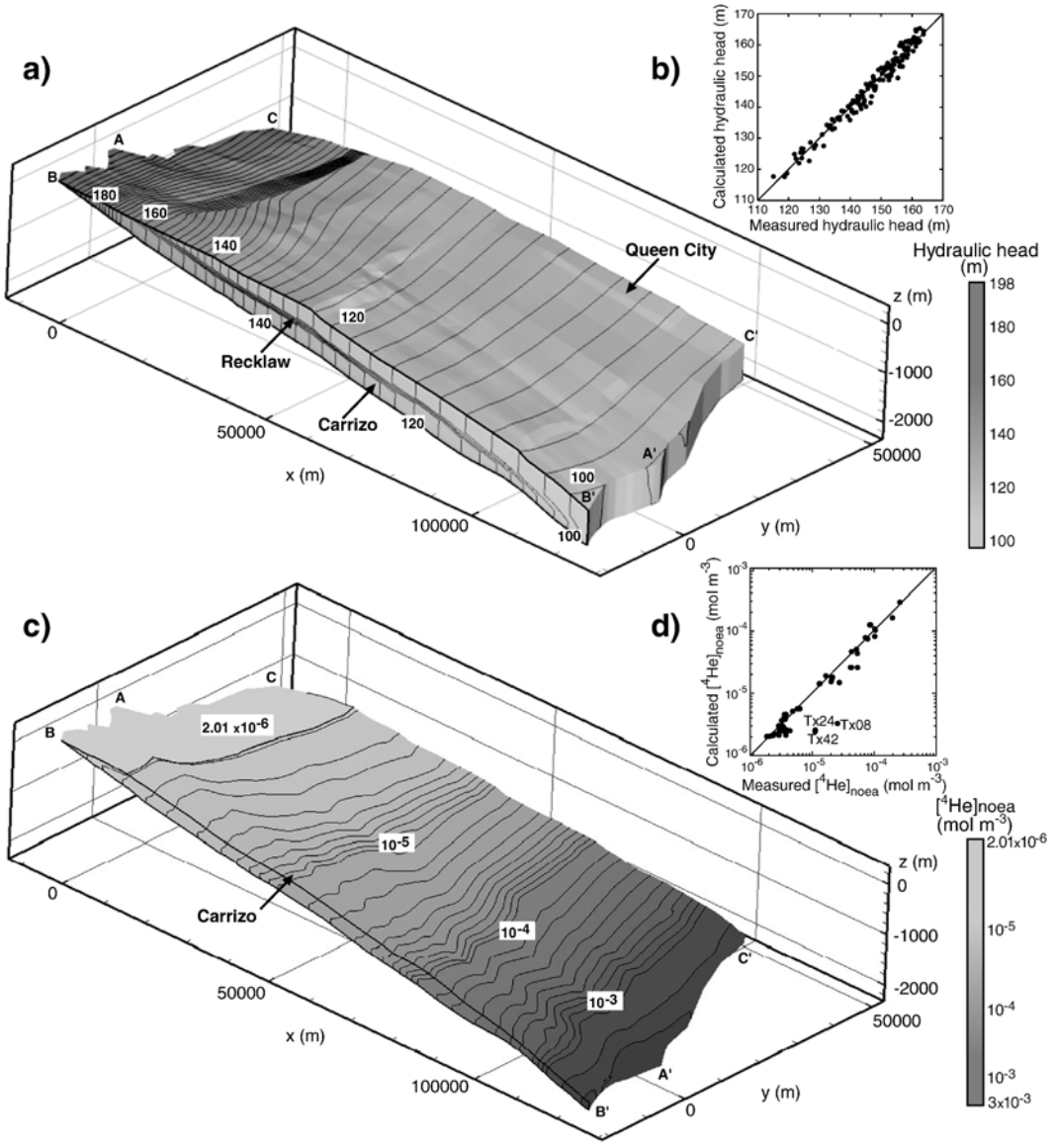

Fig. 2. a) Distribution of calculated hydraulic heads in the calibrated 3-D model; b) calculated versus measured hydraulic heads; line 1:1 plotted for reference; c) distribution of ^{4}He concentration contours (mol m^{-3}) for the 3-D calibrated transport model within the Carrizo aquifer; contour lines express constant variations of one unit inside each order of magnitude between 2×10^{-6} and 3.3×10^{-3} mol m^{-3}; d); calculated versus measured ($^4He_{noea}$) concentrations (closed circles); line 1:1 plotted for reference; outliers TX08, TX24, and TX42 are indicated.

progressive dilution on ^{4}He concentrations by recharge water present in deeper aquifers/formations. Progressive down dip increase of ^{4}He concentrations in the Carrizo is apparent (Fig. 2c). Such increase is slow near recharge areas where water movement is faster (e.g., $U\sim2.85*10^{-7}$ m s^{-1}; $x\sim10$ km) and the atmospheric component has a strong dilution effect on ^{4}He concentrations. It is faster at depth where hydraulic conductivities and thus, water velocities progressively decrease (e.g., $U\sim5.32*10^{-9}$ m s^{-1}; $x\sim50$ km), allowing for a more rapid ^{4}He accumulation due to the external flux entering the Carrizo aquifer as well as in-situ production.

Although the ^{4}He correlation coefficient is slightly lower than that of hydraulic heads, calculated and measured concentrations for the entire data set (71 measurements) are also well correlated ($r^2=0.94$; Fig. 2d). Three samples (TX08, TX24 [8,19], TX42, Fig. 2d), however, fall distinctly outside the normal ^{4}He accumulation pattern displayed in the area and cannot be

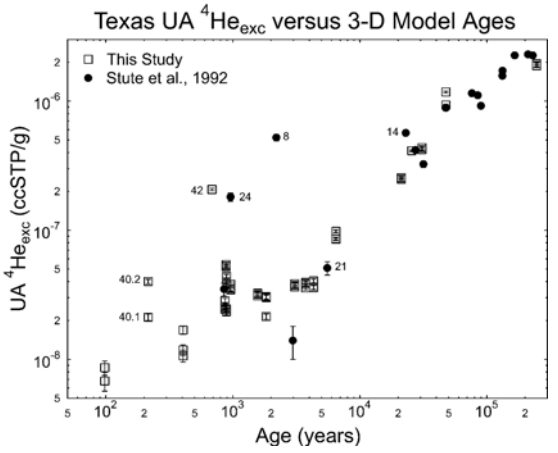

Fig. 3. $^4He_{exc}$ as a function of 3-D model ages. $^4He_{exc}$ were calculated through the UA NGT model as were those from Stute et al. [8]. Other NGT models give only slightly differing $^4He_{exc}$ values, as this parameter is very insensitive to the details of the NGT model used. All error estimates are 1σ.

reproduced by the 3-D model under realistic hydrodynamic conditions. The abnormal pattern displayed by TX08, TX24 and TX42 is readily apparent in Fig. 3, in which $^4He_{exc}$ is plotted as a function of groundwater age. Note that calculated groundwater ages, which were simulated on the calibrated 3-D groundwater flow model, account simultaneously for mixing processes due to advection, dispersion, diffusion, and cross-formational flow. Depth, not recharge distance, plays a critical role in the water age calculation. This is of particular relevance in the study area as dip and thickness of the different formations is highly variable [17], both of which are reproduced in the 3-D model. The implications of such variations together with mixing processes on the age calculation are numerous and relevant, as the age of a particular water sample will integrate its history (i.e., changes in dip, occurrence or absence of mixing) along the flow path between the recharge location and the location of a particular sample. Thus, although almost impossible to predict within such a complex 3-D velocity field, in the absence of faults, samples collected at similar recharge distances but different depths will display distinct ^4He concentrations. Typically, deeper samples will display higher ^4He concentrations (e.g., Fig. 4 [7]). The abnormal pattern displayed by TX08, TX24, and TX42 is local and can only be reproduced by a ^4He flux $\sim$ 35 times that of the calibrated model. Such high ^4He flux might occur through a local, relatively small fault, as no apparent abrupt hydraulic head changes are observed in the area. Such faults are not represented by the 3-D model. Although to a much smaller extent, samples TX14 [8,19] and TX40 also fall somewhat outside of the general pattern. These 5 outliers, however, do not in any way affect the general conclusions that follow, and will not be part of the present discussion which focus on the mid-late Holocene period. Indeed, most of the samples of our new data set (Table 2) display a young age (Fig. 3). These, together with three samples previously collected in the recharge area (TX02, TX22, TX32 [8,19]) provide us with the opportunity to address issues in relation to preservation of short climate signals, as well as observed inconsistencies between recharge area NGTs and ground temperature. Both issues are analyzed in the sections that follow.

6. Preservation of climatic signals in groundwater flow systems

6.1. Impact of dispersion — periodic versus discrete pulse signal response

To assess the impact of dispersion on the resolution of climatic records in confined aquifers, Stute and Schlosser [1] simulated the smoothing of a climatic signal through a one-dimensional approach. They concluded that high-frequency fluctuations occurring on a time scale ≤ 1 kyrs have already completely disappeared at the very beginning of the record. Among their underlying assumptions was a constant pore velocity of 1 m yr^{-1} throughout the aquifer.

Preservation of high or low frequency climatic signals is intrinsically related to the specific hydrodynamic characteristics of each individual system. Many highly productive aquifers, including the Carrizo, have far greater velocities both in the unconfined and shallow confined

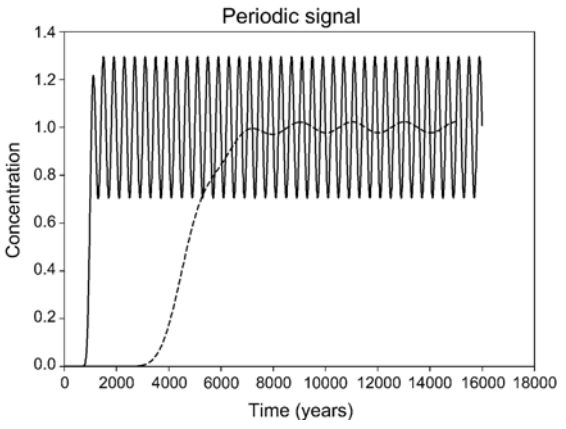

Fig. 4. Periodic signal behavior for a perturbation lasting 1 kyrs simulated under conditions adopted by Stute and Schlosser [1] (dashed line). Periodic signal behavior for a perturbation lasting only 200 yrs simulated under conditions similar to those of the Carrizo aquifer (solid line).

areas. Our 3-D model results yield a velocity of ~ 1 m yr^{-1} at a recharge distance of ~ 50 km, while an average value of ~ 20 m yr^{-1} is found within the initial 20 km from the recharge area. Values of the same order were also found through field tests (e.g., [18,36]). Note that the recharge area is composed of very permeable sandy soils [37].

We analyze the contrasting behavior of a periodic signal and that of an aperiodic discrete pulse and show that the latter can be well preserved within the Holocene in groundwater flow systems with hydrodynamic conditions similar to those of the Carrizo. Details of this analysis are presented in Appendix B. Our findings are consistent with the noble gas record in the Carrizo aquifer, which indicates an abrupt climate change at ~ 1 kyrs BP (Section 7).

6.2. Results

To compare the behavior of signals defined through different parameters, the input concentration (see Appendix B) is 1 in all cases. Similarly to the analysis by Stute and Schlosser [1], all results presented below assume an average dispersivity of 100 m. The critical parameters for a good preservation of the signal are thus the duration of the injection and the pore velocity (cf. Appendix B). Distance for which the signal will be preserved will increase with increased velocity. For a similar pore velocity, preservation of the signal will depend directly on the duration of the injection (length of climatic perturbation). The value of parameter CG, as defined in Appendix B indicates whether the signal is lost or well preserved. More specifically, our simulations show that the signal is almost entirely lost for CG=2.5, while extremely sharp for CG=5.

We tested preservation of the signal under assumptions adopted by Stute and Schlosser [1], i.e., V=1 m yr^{-1} and T=2 kyrs (perturbation of 1 kyrs). For example, our results show that for a distance of 5 km (5 kyrs) CG=2.8. CG values decrease as age and distance increase. Our results thus confirm findings by Stute and Schlosser [1] which indicate that a periodic climatic perturbation lasting ≤1 kyrs will be lost at the very beginning of the record. Fig. 4 clearly illustrates the loss of signal under these conditions. Our simulations also show that in order for a periodic climatic signal to be well preserved at a distance of 20 km (e.g., LGM) under similar conditions, a perturbation lasting ~ 3.5 kyrs (CG~5) would be required. This behavior greatly contrasts with preservation of a much shorter periodic signal (T=400 yrs) in a groundwater flow system with an average velocity of 20 m yr^{-1} (e.g., Carrizo). Under these conditions it is apparent that a periodic climatic perturbation of 200 yrs remains perfectly sharp and visible for time scales of one thousand years (CG=5.7) and beyond (Fig. 4).

As stated earlier, however, behavior of a discrete signal (e.g., abrupt climate change) greatly contrasts with that of a periodic one. Fig. 5a, which shows the behavior of a distinct, discrete signal under assumptions by Stute and Schlosser [1] illustrates this contrast in a clear fashion. Indeed, under such conditions, a climatic perturbation of 1 kyrs, although of reduced amplitude (four fold), remains perfectly identifiable 5 kyrs later and beyond. Although of much smaller amplitude it is apparent that such a peak is still present 50 kyrs later. Similarly, it is clear that a much shorter perturbation (200 yrs) remains extremely sharp and of much greater amplitude (~ 2 fold reduction) 1 kyrs later under conditions mimicking those of the Carrizo (Fig. 5b). It is apparent that this short perturbation remains strong and visible for thousands of years and it is still well defined 10 kyrs later (Fig. 5b).

Because our noble gas climatic record in Texas indicates an abrupt change in climatic conditions at around 1 kyrs, we

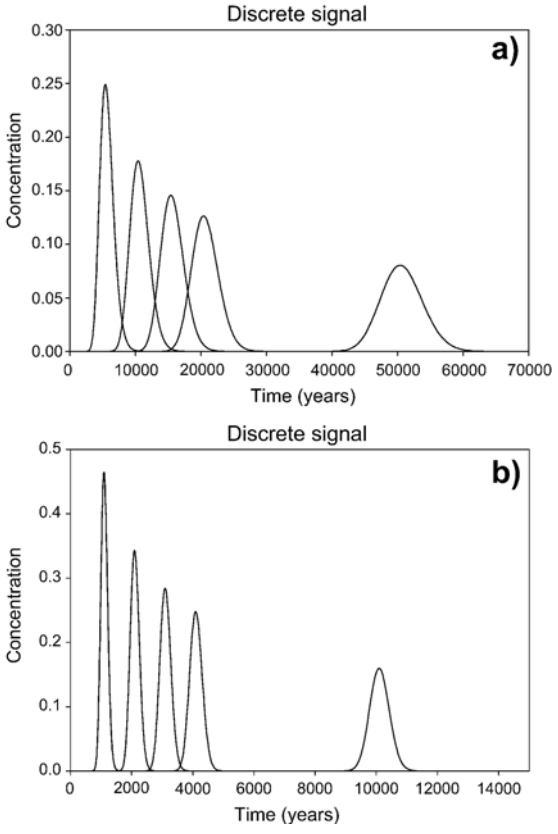

Fig. 5. a) Behavior of a discrete signal (e.g., abrupt climate change) for a perturbation lasting 1 kyrs simulated under conditions adopted by Stute and Schlosser [1]. Peaks at 5, 10, 15, 20, and 50 kyrs are indicated; b) behavior of a discrete signal (e.g., abrupt climate change) for a perturbation lasting only 200 yrs simulated under conditions similar to those of the Carrizo aquifer. Peaks at 1, 2, 3, 4, and 10 kyrs are indicated.

were interested in investigating the potential duration of such an abrupt perturbation for which a climatic signal might still be preserved. Our simulations indicate that while a short 100 yr periodic perturbation has been almost entirely lost at 1 kyrs (CG=2.8), a discrete 100 yr perturbation remains clearly visible and well defined.

In the sections that follow we discuss our NGT record in Texas, with particular emphasis to the mid-late Holocene period (≤ ~ 6 kyrs).

7. Noble gas temperature (NGT) record

7.1. UA NGT model results

Fig. 6 shows our site-averaged NGT values together with those of Stute et al. [8] plotted as a function of 3-D model ages. All NGTs were calculated using the standard unfractionated air (UA) model [1] for incorporation of excess air. A χ^2 test (MSWD>3) was performed for replicates of each individual site (Table 2). Because potential laboratory or sampling problems typically lead to underestimation of noble gas concentrations (e.g. leaks, incomplete outgassing) and thus, erroneously high NGTs, highest NGT replicates were removed from a number of sites that did not pass the χ^2 test (MSWD>3; see also [38]). A new average from the remaining runs was then recomputed. Only 8 runs out of 49 were removed and 16 out of our 20 sites have averages from at least 2 runs (total of 41 runs).

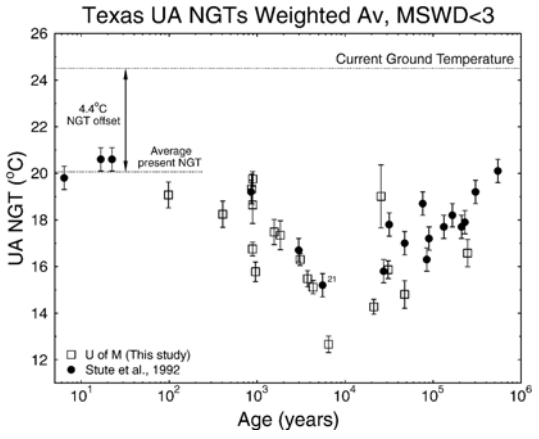

Fig. 6. UA model NGTs vs 3-D model groundwater ages. For data from this study, points are site-averaged values using the procedure outlined in the text. NGTs from Stute et al. [8] were calculated manually from Ne, Kr and Xe data. Current ground temperature and average present NGTs are indicated and display an offset of 4.4 °C. Average present NGT value was calculated using TX02, TX22, and TX32 [8,19] together with TX39 (this study, Table 2), all of which are located in the recharge area.

Although argon was discarded from NGT estimations by Stute et al. [8], it is apparent that a very good general agreement between both data sets is present (Fig. 6). The NGT record shows a general pattern of increasing temperatures with decreasing age between ~ 6 kyrs BP and present, from 12.66 °C to an average of 20.06 °C, i.e., a NGT rise of 7.4 °C within the Holocene alone. This NGT trend is abruptly interrupted at ~ 1 kyrs BP, a time during which an abrupt change in climatic conditions occurred (Section 7.3). A gap between 6 and >21 kyrs is present in the NGT record indicating that the LGM has not yet been captured in this system, a conclusion very different from Stute et al. [8] (see also [13]). Samples >21 kyrs belong mostly to previously published data and will not be part of the present discussion.

The most immediate striking feature in Fig. 6 relates not to the NGT record per se, but rather, to the significant 4.4 °C offset displayed between present UA NGTs (20.06 °C) and ground temperature (24.5 °C). Ground temperature was estimated based on 42 available Carrizo water table temperature measurements in the study area [12,39]. A basic requirement for a correct application of the noble gas thermometer is that noble gases should closely record the ground temperature at the interface with the saturated zone [1–4].

Bias to low NGTs in the Carrizo recharge area is not an isolated case. Bolchot, Germany [4], and southern Michigan [9,10] are among groundwater systems sharing similar bias. Clearly, none of the standard NGT estimation models fully describe all the mechanisms controlling noble gas concentrations and thus, resulting NGTs in these areas. Under these circumstances, no meaningful NGT paleoclimatic reconstruction is possible. We thus address this issue prior to further discussing the NGT paleoclimate record in the Carrizo. Unfortunately, noble gas data used by Stute et al. [8] to construct the Carrizo NGT record has not been published and it is not available to us. Thus, the in-depth analysis that follows is based almost entirely on our new data set (Table 2).

7.2. NGT bias to ground temperature

In addition to the misfit between modern UA NGTs and average ground temperature, a systematic and significant offset between model UA NGT noble gas concentrations and the actual measured values is also observed. Indeed, total χ^2=201.6 for 82 degrees of freedom for the 41 replicates, reflecting significant difficulties of the UA model to describe this data set. A similar analysis using the continuous equilibration (CE) model of Aeschbach-Hertig et al. [11] yields χ^2=65.3 for 41 degrees of freedom which illustrates its inability to

adequately fit the Carrizo data set. Compounding this problem are the severe non-uniqueness issues of the CE model leading to systematic large parameter uncertainties and, occasionally, a complete inability to estimate certain parameters, and thus, corresponding NGTs (e.g., [5,10]). A plot (not shown) of CE NGTs versus 3-D model ages displays a similar trend to that of UA NGTs. Although CE NGTs are ~ 1 °C above UA NGTs, the former remain biased to low recharge NGTs by > ~ 3 °C.

An alternative NGT model by Mercury et al. [14] explains noble gas misfits by invoking changes in solubility due to negative water pressure in the capillary zone. A minimum $\chi^2 = 198.8$ was found at a single assumed pressure of −36 bars, with 80 degrees of freedom. This χ^2 value is only slightly better than that for the UA model. Although recharge NGTs did increase by ~ 1.9 °C, a 2.5 °C offset with respect to ground temperature remains.

All NGT models assume that the ASW component is incorporated at the water table which is in contact with standard air at the normal atmospheric pressure (P_{atm}) corresponding to the altitude of a particular recharge area. Hall et al. [10] suggested that noble gas partial pressures at the interface with the water table are higher than predicted from standard air, possibly due to net depletion of O_2 resulting from biological processes such as respiration. These authors called an NGT system which allows for higher noble gas pressures the "oxygen depletion" (OD) model. They demonstrated that not only is χ^2 improved over that of the UA model, it also leads to an almost perfect fit of the actual ground temperature, thus, eliminating the NGT offset. Build up of CO_2 in the gas phase can be suppressed via CO_2 solubility and/or conversion into bicarbonate. For example, Tan [40] estimated that typical subsoil air (depth of 1.2 m) in temperate zones during winter time has a total O_2 plus CO_2 content of only 10.3%. Air with this composition would have 1.115 times the normal partial pressure for noble gases. Higher values are likely to be present closer to the water table.

A similar χ^2 analysis using the OD model was conducted. Fig. 7a, b shows how each individual noble gas component behaves as a function of the overpressure factor. While Ne and Kr are reasonably well fit over most of the pressure range, the opposite is true with Ar and Xe. Ar is too high at normal pressure while Xe is too low. Only at pressures > $1.1P_{atm}$ do all four gases fit reasonably well. The minimum χ^2 was found for an overpressure factor of 1.14 corresponding to a combined O_2 and CO_2 air content of 8.7% as opposed to the expected value of 21%. This corresponds to an NGT increase of 4.6 °C for sample TX39c located in the recharge area, leading to an NGT of 23.7 °C, just below the average ground temperature. It is interesting to note that the minimum χ^2 is 113.0 for 81 degrees of freedom. Thus, with a MSWD = 1.40, the OD model actually performs better than the CE model (MSWD = 1.59). This is of particular significance as while one single additional parameter was used for the OD model, 41 additional parameters were required for the CE model, further reinforcing the notion that the OD model, in addition to better parameter estimation performance, better represents actual recharge conditions than the CE model. Consequently, the discussion that follows on the Carrizo NGT record is based on OD model results and comparison between these and UA NGT results.

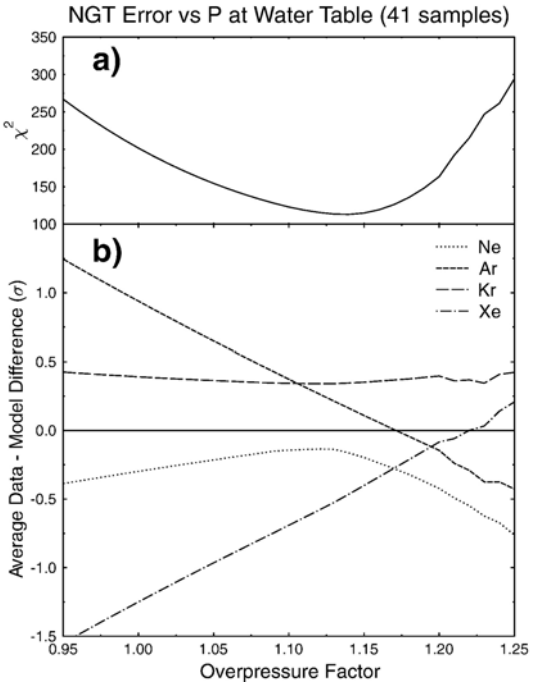

Fig. 7. OD model analysis for the 41 Carrizo samples from this study plotted in Fig. 6 (see also Table 2); a) overall χ^2 as a function of overpressure factor. This is the relative amount of noble gas compression due to water loading during infiltration and/or the reduction of active gases due to processes occurring in the unsaturated zone; b) a plot of the average misfit (in units of 1σ) of the different noble gases as a function of overpressure factor. For a factor of 1 (equivalent to the UA model), there is significantly more measured Ar and less Xe than predicted from the model. As the overpressure factor is increased, the noble gas misfits converge toward zero, with a χ^2 minimum at 1.14. The model is constrained so that excess air for any individual analysis is non-negative.

7.3. Combined NGT and excess air Holocene record

The overall NGT shift observed between the UA and OD models for an overpressure factor of 1.14 is ~ 4.7 °C. Fig. 8 shows the UA and OD NGT record plotted as a function of 3-D model ages. As expected, recharge OD NGTs very closely reproduce ground temperature.

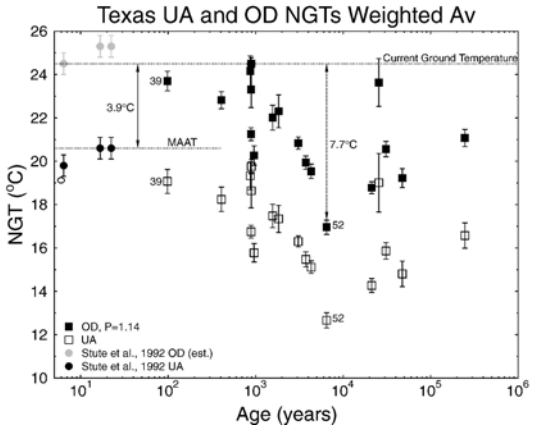

Fig. 8. Site averaged UA and OD models, the latter with a pressure factor of 1.14. The youngest samples near the recharge zone reproduce actual present day ground temperatures. OD model values for recharge area samples (TX02, TX22, TX32 [8]) were estimated by averaging the offset between UA and OD model NGTs for the youngest samples from this study. The MAAT and current ground temperature in the Carrizo recharge area are indicated and display an offset of 3.9 °C.

Of relevance is the observed OD 7.7 °C NGT increase between 6 kyrs BP (TX52) and present time. Such a significant NGT increase within the Holocene alone is spectacular, yet real. It is documented by multiple high quality replicates (30) and it represents, to our knowledge, the best documented noble gas data set for such a short time period. It is also apparent that this wealth of data blends particularly well with previously published data (Fig. 6). Of significance, is sample TX21 (UA NGT = 15.2 °C) for which the conclusion that the LGM was 5 °C lower than present was based [8]. TX21 with a 3-D model age of ~ 5.5 kyrs (Fig. 3) and a very similar ^{14}C age [7,19], definitely belongs to the Holocene period, not to the LGM (see also [13]). Previous LGM identification in the Carrizo aquifer by Stute et al. [8] was based solely on the identification of an important NGT cooling (≥ 5 °C) with respect to the present.

The significant 7.7 °C NGT Holocene change raises two critical questions: a) what is the noble gas thermometer precisely recording in the recharge area?; b) what is the exact meaning of such major NGT changes? These are addressed below.

Another striking feature of this NGT Holocene record is the presence of an extremely disturbed period between ~ 0.9 and 1 kyrs BP during which NGT shifts of over 4 °C are observed. As demonstrated in Section 6, discrete, short (100–200 yrs) high-frequency climatic signals are expected to be extremely well preserved in the Carrizo. Parallel to this NGT record is yet another striking feature as evidenced by the amount of entrapped excess air as a function of model ages (Fig. 9). Indeed, UA and OD model excess air values show equally abrupt changes within the same period. The record is represented by a dramatic excess air increase from ~ 1 to ~ 0.9 kyrs BP. Low to almost non-existent entrapped excess air is in place ≥1 kyrs BP, while high excess air amounts dominate the last millennium.

The Holocene NGT record is very clear. It shows the presence of a cool climate prior to 1 kyrs BP, as opposed to a warmer one following the transition, and a highly disturbed period at ~ 1 kyrs. Present climate in the study area is warm (MAAT is 20.6 °C) and semi-arid. The abrupt climatic NGT perturbation at ~ 1 kyrs thus marks the transition between a cool and warm regime. The excess air record is complementary to that provided by NGTs and gives information on the type of regime in place. More specifically, our data undoubtedly shows that high amounts of entrapped excess air are associated with arid/semi-arid regimes and episodic aquifer recharge. Below, we will further argue that low or non-existent excess air is indicative of humid regimes. We thus associate our combined NGT and excess air record with a cooler and wet regime ≥1 kyrs BP, in contrast to a warm, semi-arid one at < 1 kyrs BP.

The occurrence of an abrupt climatic transition at ~ 1 kyrs BP in low latitude areas has been extremely well documented, including regions close to our study area. For example, in Texas and Oklahoma it has been documented in great detail through channel incision and

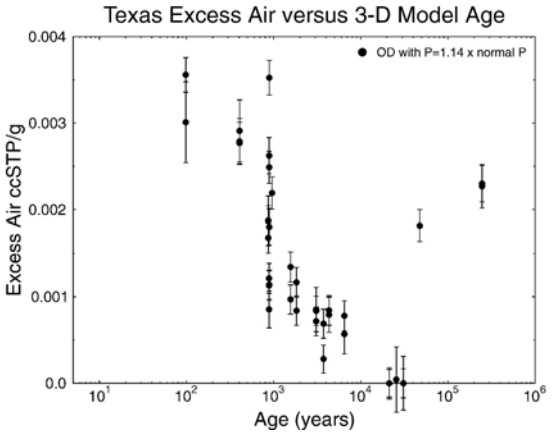

Fig. 9. Excess air for the OD model versus groundwater age. OD model excess air is significantly lower than that for the UA model, essentially disappearing at ~ 6 kyrs BP. The dramatic excess air increase at ~ 1 kyrs BP and minimum at ~ 6 kyr BP correspond to a transition period from a cooler wetter period to a warmer, semi-arid one as recorded in multiple paleoclimate records from southern Texas and neighboring areas around the Gulf of Mexico.

flood plain abandonment of rivers (e.g., [41,42]). Further south, in the Yucatan Peninsula, oxygen isotopes and gypsum records from lake sediments indicate the occurrence of an extremely disturbed period at ~ 0.8–1 kyrs BP [43,44]. This period is believed to be the driest of the mid-late Holocene, which also coincided with the collapse of the Classic Maya civilization [45]. The Maya were highly dependent on rainfall and surface reservoirs as their main source of water supply.

7.4. High and low excess air versus arid and humid climate regimes

A negative relationship between excess air and precipitation was previously identified in the UK [46]. In addition, a relationship between high excess air and tropical aquifers was also suggested, potentially in relation to large water table fluctuations [38]. A similar finding was noted by Mercury et al. [14] for a NGT record from Brazil and they were also able to correlate the quantity of apparent excess air with humidity via their fitted capillary pressure values. It now appears that the apparent quantity of excess air present in a sample, no matter what NGT estimation scheme is used, is a significant indicator of past climate. To understand the connection between excess air content and climate regimes, it is critical to understand the overall functioning of the hydrologic system in question (e.g., [15]).

Present semi-arid climate in our study area is characterized by a severe moisture deficit, with an average annual evaporation rate ~ 3 times that of rainfall (~ 650 mm yr^{-1} [23]). Precipitation is heaviest in May–June, lowest in January–March. The drainage system, characterized by intermittent flow [47], reflects both the precipitation regime and high temperatures in the area. Under these conditions, recharge of the Carrizo (~ 145 mm yr^{-1}, this study, see also [23]) is likely to be mostly provided through flood flows and stream-channels [37] when the drainage system is activated due to major storms (e.g., Gulf of Mexico hurricanes). Present average water table depth in the Carrizo is 25.4 m [39].

Based both on climate and hydrological conditions currently in place in the area as well as our Carrizo data set, we conclude that high excess air content is associated with relatively deep water table levels. These, in turn, are commonly linked to arid/semi-arid climates which are generally characterized by discontinuous recharge, typically associated with discrete episodes of strong rainfall. Such episodes lead to significant fluctuations of the water table, and consequently, to incorporation of high excess air amounts [28]. By contrast, humid regimes (warm or cool) which are typically characterized by continuous annual precipitation, very shallow water table, and thus, absence of major water table fluctuations, are expected to be characterized by low excess air. Thus, our combined NGT and excess air record strongly suggests that while the last millennium has been characterized by a warm and arid/semi-arid climate, conditions in the mid-late Holocene (1–6 kyrs BP) were wetter and cooler as evidenced by the small to almost non-existent excess air amounts. The presence of a wetter period >1 kyrs BP is also supported by a diversity of proxies (e.g., [41]). We thus conclude that the ~ 1 kyrs transition period translates into a dramatic drop of the water table level in the Carrizo aquifer. Such a dramatic water table drop has critical implications on the information presently being recorded by the noble gas thermometer in the Carrizo recharge area. These are discussed below.

7.5. Reading the noble gas thermometer in the Carrizo recharge area

Prior to ~ 1 kyrs BP our combined NGT and excess air record indicate a cool humid climate in which the water table is expected to be close to the surface. Thus, throughout most of the mid-late Holocene (1–6 kyrs BP), NGTs are recording ground temperature changes which result directly from atmospheric variations. The opposite is true at present time and throughout most of the last millennium, which differs from conclusions in Castro and Goblet [13]. Indeed, ground temperatures reflecting atmospheric variations are expected to be within ~ 1 °C that of MAAT [8,48]. Ground temperature of the Carrizo at the water table is 3.9 °C above the MAAT (Fig. 8) and clearly independent of present climatic atmospheric conditions. Instead, due to the significant water table depth, it is a direct reflection of heat flow in the region. Impact of heat flow in the water table/ground temperature is also evidenced by the rather homogeneous temperature in the unconfined Carrizo at all depths [12]. Consequently, present NGTs are recording ground, not surface conditions. The observed NGT increase of over 4 °C during the transition period reflects mostly the drop of the water table due to a change from humid to semi-arid regime rather than a real atmospheric temperature change. Consequently, in order to obtain an approximate absolute temperature change through the NGT record during the Holocene (~ 6 kyrs BP), ~ 3.9 °C corresponding to the current temperature difference between the ground and MAAT have to be subtracted. If one discards any potential seasonal influence on aquifer recharge, temperature change between 6 kyrs BP (TX52) and present would thus be 3.6 °C. However, numerous general circulation models (GCMs [49–52]) indicate that while current climate has

Table 3
Parameters used in groundwater flow, ^{4}He transport simulations, and direct simulations of water age

Symbol	Description	Values					Units
		Water	Queen	Recklaw	Carrizo	Wilcox	
h	Hydraulic head	Computed					m
z	Elevation above datum (sea level)						m
$\bar{\bar{K}}$	Hydraulic conductivity tensor	Computed					m s^{-1}
	Initial K values (outcrop)		2.94E− 4	1.7E− 8	3.5E− 4	1.09E− 11	m s^{-1}
S_s	Specific storage coefficient		9.9E− 5	9.8E− 4	1.0E− 4	9.8E− 4	m^{-1}
$\bar{\bar{\alpha}}$	Dispersivity tensor composed of α_{L1}, α_{L2} and α_T	$\bar{\bar{D}} = \bar{\bar{\alpha}}\, U$					m
α_{L1}, α_{L2}	Longitudinal dispersivity	125					m
α_T	Transversal dispersivity	12.5					m
U	Darcy velocity	Computed					m s^{-1}
ω	Porosity		20.0	12.5	35.0	26.0	%
q_m	Source term of mass of tracer						mol m^{-3} s^{-1}
C	^{4}He concentration	Computed					mol m^{-3}
d	^{4}He diffusion coefficient (58 °C) [15]		1.3E− 9	6.7E− 10	1.3E− 9	6.7E− 10	m^2 s^{-1}
d	$^1H^3H^{16}O$ diffusion coefficient [7]		3.8E− 10	1.9E− 10	3.8E− 10	1.9E− 10	m^2 s^{-1}
ρ	Reference water density	1000					kg m^{-3}
V	Horizontal pore velocity						m s^{-1}
t	Time						s
θ	Age	Computed					s

nearly the minimum seasonality between summer and winter insolation for the Northern Hemisphere, seasonality was at its maximum at the mid-Holocene optimum (~ 6 kyrs BP). Most GCMs predict warmer summers and cooler winters at ~ 6 kyrs BP. Vettoretti et al. [50] GCM model further indicates a significant rise in the precipitation/evaporation ratio for Southern Texas during this period, strongly suggesting that effective recharge in the Carrizo at ~ 6 kyrs BP occurred mostly during winter. Winter recharge in the Carrizo in the early to mid-Holocene will greatly enhance NGT absolute differences with respect to present. Thus, real atmospheric temperature changes between ~ 6 kyrs BP and present are likely much smaller than the suggested 3.6 °C when seasonality is discarded. This seasonality impact on Holocene NGTs is consistent with findings by Vettoretti et al. [50] which predicted relatively small annual air and sea surface temperature changes for Southern Texas at ~ 6 kyrs BP with respect to present. Our NGT and excess air records also indicate small temperature changes in the last millennium.

8. Summary

Through a combination of 3-D simulations of groundwater flow, ^{4}He transport, and groundwater ages as well as a comparative analysis of both, impact of dispersion on high frequency climatic signals and assumptions underlying competing NGT models, we address some basic issues in relation to the use of the noble gas thermometer in groundwater flow systems. Our analysis is based on the combined previously published [8,19] and new (this study) data sets. Our combined analysis indicates that samples previously attributed to the LGM [8] belong to mid-late Holocene.

It is also shown that groundwater flow systems, at least those with similar characteristics to that of the Carrizo aquifer, do have the ability to preserve short term climatic fluctuations (100–200 yrs) archived by noble gases. Abrupt climate shifts during the late Holocene, which are associated with significant NGT changes ($\geq$ 5 °C) do not reflect equally important changes in the MAAT. Rather, these reflect the combined effect of atmospheric temperature changes, seasonality of recharge and, above all, important variations of water table depth which result from shifts between cold and humid versus warm and arid regimes. The excess air component appears to play a critical role in identifying such climatic shifts. Specifically, the Carrizo combined data set indicates an abrupt shift from a cool, humid regime to a warmer, arid one at ~ 1 kyrs BP. A major Holocene NGT change of 7.7 °C with respect to present now identified is mostly the result of a dramatic water table drop which took place during the ~ 1 kyrs BP transition period. Current NGTs in the Carrizo recharge area do not appear to be recording atmospheric changes. Rather, these are recording ground conditions reflecting mostly the impact of heat flow in the area.

Observed systematic bias to low UA and CE NGTs in recharge areas can be reconciled through NGT estimation models which account for a noble gas partial pressure

increase in the unsaturated zone, potentially due to O_2 depletion (OD model, [10]).

Acknowledgments

The authors wish to thank an anonymous reviewer for his/her constructive comments as well as Dr. R. van der Hilst for the editorial handling of this manuscript. The authors also thank E. T. Baker (USGS, Austin), J.-P. Nicot (Bureau of Economic Geology, Austin), R. E. Mace, G. Franklin, J. Hopkins (Texas Water Development Board, Austin), as well as L. Ackers, M. Mahoney, J. West, and C. Gonzales (Evergreen Underground Water Conservation District, Pleasanton) for their help in providing additional geological and hydrogeological information as well as assistance with field sampling. Financial support by the U.S. National Science Foundation grant EAR-03087 07 is greatly appreciated.

Appendix A

A.1. 3-D Model

A.1.1. Mathematical formulation and numerical approach

To model groundwater flow and mass transport, two classical equations are solved. For incompressible fluids, the general 3-D diffusion equation is expressed as [31]:

$$\nabla\cdot\left(\bar{\bar{K}}\,\nabla h\right) = S_s\frac{\partial h}{\partial t} \tag{1}$$

where $\bar{\bar{K}}$ is the hydraulic conductivity tensor, h is the hydraulic head, S_s is the specific storage coefficient, and t is the time. All symbols and values used in this section are defined in Table 3.

To account for advection, kinematic dispersion, and molecular diffusion the 3-D transport equation is expressed as:

$$\nabla\cdot\left(\left(\bar{\bar{D}}+\omega\,\bar{\bar{d}}\right)\nabla C - C\,\vec{U}\right) = \omega\frac{\partial C}{\partial t} + q_m \tag{2}$$

where $\vec{U}$ is the Darcy velocity, $\bar{\bar{d}}$ is the pore diffusion coefficient tensor of the solute in question, ω is the porosity, q_m is a source term corresponding to the added or withdrawn mass of tracer per unit volume per unit time, and C is the concentration of the solute in water. $\bar{\bar{D}}$ is the dispersivity coefficient tensor.

Movement of water in porous media is, in addition to advection and like any other tracer, also affected by kinematic dispersion, molecular diffusion, and cross-formational flow (e.g., [7,32,33]). 3-D groundwater age simulations taking these processes into account were carried out in steady-state and calculated as follows [32]:

$$\nabla\cdot\left(\left(\bar{\bar{\alpha}}\,U+\omega\,\bar{\bar{d}}\right)\nabla\theta - \theta\vec{U}\right) = \omega \tag{3}$$

where θ is the age.

All simulations were conducted with the finite element code METIS [34] in steady-state.

A.1.2. Boundary conditions, calibration data and parameter values

Groundwater flow boundary conditions include hydraulic heads prescribed on the outcrop areas of all formations as well as on top of the Queen City aquifer obtained through geostatistical modeling [17]. A no-flow boundary condition was imposed both at the base of the Wilcox and lateral boundaries of the domain. In addition, a hydraulic conductivity of 10^{-5} m s^{-1} was imposed in the Wilcox Geothermal Corridor area, allowing the water to be evacuated upward, reflecting the situation occurring at the major growth–fault system.

For the transport model an ASW ^{4}He concentration of $2.01 * 10^{-6}$ mol m^{-3} was imposed on all outcrop areas. On top of the Queen City an outlet condition was prescribed, which allows ^{4}He to be evacuated upward by advection. A ^{4}He flux representing the external contribution from the underlying crust and/or mantle was imposed at the base of the Carrizo. This upward external flux is our ^{4}He transport calibration parameter. Inside the domain, a term representing in-situ ^{4}He production was imposed (cf., [12]).

To account for groundwater mixing, water age is treated in a similar manner to that of a solute concentration. Water age is simulated by considering the product of water mass (ρV) and age (θ) [32], where ρ is the water density and V is the water volume. This quantity, referred to as "age mass", is conserved and is equivalent to moles of a solute tracer. Boundary conditions included zero-age mass flux across all no flow and inflow boundaries of the 3-D domain (Fig. 1b) and no age–mass dispersive flux across outflow boundaries.

Appendix B

B.1. Periodic versus discrete pulse signal response — mathematical formulation

The analysis presented below is not exhaustive and remains greatly simplified. A more thorough analysis on the impact of dispersion on high versus low frequency climatic signals will be presented elsewhere.

We start by analyzing a periodic signal behavior, for example, a fluctuation of noble gas concentrations in the water table translating into NGT variations. Here, we deal with a succession of peaks separated by a constant time interval T (period). As time since the initial pulse increases, partial superposition of the peaks will occur, leading to smoothing and eventually a loss of signal. We analyze this periodic signal behavior in a mono-dimensional (along x) groundwater flow system. The dispersion equation is described by:

$$D\frac{\partial^2 C}{\partial x^2} - V\frac{\partial C}{\partial x} = \frac{\partial C}{\partial t} \tag{5}$$

where V is the horizontal pore velocity. The solution to a brief pulse (injection) is given by:

$$C(x,t) = \frac{m}{2\varepsilon\sqrt{\pi Dt}}\exp\left(-\frac{(x-Vt)^2}{4Dt}\right). \tag{6}$$

Where m is the initial mass of the solute and ε kinematic porosity. This gaussian distribution can be described by the width corresponding to the half-height of the peak concentration ($C_{max}/2$) at a time t, here referred to as half-width. For example, if $\exp\left(-\frac{1^2}{4Dt}\right) = 0.5$, half-width $= 3.4\sqrt{Dt}$. Two pulses sent within a time interval T will remain separated only if the sum of their half-widths is much smaller than the distance between their maxima (VT). This requirement for a proper preservation of the signals can be expressed in terms of the dimensionless number CG as follows:

$$\mathrm{CG} = \frac{VT}{\sqrt{Dt}} = \frac{VT}{\sqrt{\alpha Vt}} = \frac{VT}{\sqrt{\alpha L}} \tag{7}$$

where L is the distance covered by the signal. Note that $(\mathrm{CG})^2$, in addition to T^2/t which directly relates the signal period to the time since the first pulse occurred, incorporates also D/V^2, the parameter on which Stute and Schlosser [1] based their analysis. Incorporation of T^2/t renders CG dimensionless, thus, ideal for analysis of the signal's behavior. To identify the CG threshold values for which the peak of a particular signal remains sharp, and that one for which it blends with neighboring signals, the response to a sinusoidal injection was simulated. The latter is given by the convolution integral:

$$C(x,t) = \int_0^t I(\tau)\frac{1}{2\varepsilon\sqrt{\pi D(t-\tau)}}\exp\left(-\frac{(x-V(t-\tau))^2}{4D(t-\tau)}\right)\mathrm{d}\tau \tag{8}$$

where τ is time and $I(\tau)\mathrm{d}\tau$ is the tracer mass injected during time interval $\mathrm{d}\tau$:

$$I(t) = V\varepsilon(v_m + v_a \times \sin(2\pi t/T)) \tag{9}$$

where $V\varepsilon$ is the water flux, and v_m and v_a are the average and amplitude of the signal's fluctuation. Note that this sinusoidal signal is smoother than the succession of pulses discussed above. After a certain distance, however, the shape of a short signal displays little dependence on its initial shape. Our simulations show that the signal is almost entirely lost for CG=2.5, while extremely sharp for CG=5.

Behavior of a discrete high-frequency pulse signal (e.g., an abrupt change in climate) is distinct and contrasts greatly with that one of a periodic signal. To observe its propagation over time a similar approach was used in which the signal corresponds to half a period, i.e., $T/2$.

References

[1] M. Stute, P. Schlosser, Principles and applications of the noble gas paleothermometer, in: P.K. Swart, K.C. Lohmann, J.A. McKenzie, S. Savin (Eds.), Climate Change in Continental Isotopic Records, Geophysical Monograph, vol. 78, AGU, 1993, pp. 89–100.

[2] M. Stute, P. Schlosser, Atmospheric noble gases, in: P.G. Cook, A.L. Herczeg (Eds.), Environmental Tracers in Subsurface Hydrology, Kluwer, Dordrecht, 1999, pp. 349–377.

[3] R. Kipfer, W. Aeschbach-Hertig, F. Peeters, M. Stute, Noble gases in lakes and ground waters, Noble Gases in Geochemistry and Cosmochemistry, Rev. Min. and Geochem., vol. 47, Mineralogical Society of America, Washington, D.C., USA, 2002, pp. 615–700.

[4] M. Stute, C. Sonntag, Palaeotemperatures derived from noble gases dissolved in groundwater and in relation to soil temperature, Panel Proceedings Series STI/PUB/859, IAEA, 1992, pp. 111–122.

[5] W. Aeschbach-Hertig, M. Stute, J.F. Clark, R.F. Reuter, P. Schlosser, A paleotemperature record derived from dissolved noble gases in groundwater of the Aquia Aquifer (Maryland, USA), Geochim. Cosmochim. Acta 66 (5) (2002) 797–817.

[6] F.M. Phillips, M.C. Castro, Groundwater dating and residence-time measurements, in: J.I. Drever (Ed.), Surface and Ground Water, Weathering, and Soils, Treatise on Geochemistry, vol. 5, Elsevier, Oxford, UK, 2003, pp. 451–497.

[7] M.C. Castro, P. Goblet, Calculation of ground water ages — a comparative analysis, Ground Water 43 (3) (2005) 368–380.

[8] M. Stute, P. Schlosser, J.F. Clark, W.S. Broecker, Paleotemperatures in the Southwestern United States derived from noble gases in ground water, Science 256 (5059) (1992) 1000–1001.

[9] L. Ma, M.C. Castro, C.M. Hall, A late Pleistocene–Holocene noble gas paleotemperature record in southern Michigan, Geophys. Res. Lett. 31 (23) (2004) L23204, doi: 10.1029/2004GL021766.

[10] C.M. Hall, M.C. Castro, K.C. Lohmann, L. Ma, Noble gases and stable isotopes in a shallow aquifer in southern Michigan: implications for noble gas paleotemperature reconstructions for cool climates, Geophys. Res. Lett. 32 (18) (2005) L18404, doi: 10.1029/2005GL023582.

[11] W. Aeschbach-Hertig, F. Peeters, U. Beyerle, R. Kipfer, Paleotemperature reconstruction from noble gases in ground water taking into account equilibration with entrapped air, Nature 405 (6790) (2000) 1040–1044.
[12] M.C. Castro, D. Patriarche, P. Goblet, 2-D numerical simulations of groundwater flow, heat transfer and ^{4}He transport — implications for the He terrestrial budget and the mantle helium–heat imbalance, Earth Planet. Sci. Lett. 237 (3–4) (2005) 893–910, doi: 10.1016/j.epsl.2005.06.037.
[13] M.C. Castro, P. Goblet, Noble gas thermometry and hydrologic ages: evidence for late Holocene warming in Southwest Texas, Geophys. Res. Lett. 30 (24) (2003) 2251, doi: 10.1029/2003GL018875.
[14] L. Mercury, D.L. Pinti, H. Zeyen, The effect of the negative pressure of capillary water on atmospheric noble gas solubility in ground water and palaeotemperature reconstruction, Earth Planet. Sci. Lett. 223 (1–2) (2004) 147–161, doi: 10.1016/j.epsl.2004.04.019.
[15] G. Favreau, A. Guero, J.L. Seidel, Comment on "Improving noble gas based paleoclimate reconstruction and groundwater dating using ^{20}Ne/^{22}Ne ratios," by F. Peeters et al. Geochim. Cosmochim. Acta 67 (2003) 587–600;
Geochim. Cosmochim. Acta 68 (6) (2004) 1433–1435, doi: 10.1016/j.gca.2003.07.022.
[16] M.C. Castro, P. Goblet, Calibration of regional groundwater flow models: working toward a better understanding of site-specific systems, Water Resour. Res. 39 (6) (2003) 1172, doi: 10.1029/2002WR001653.
[17] D. Patriarche, M.C. Castro, P. Goblet, Large-scale hydraulic conductivities inferred from three dimensional groundwater flow and ^{4}He transport modeling in the Carrizo aquifer, Texas, J. Geophys. Res. 109 (B11) (2004) B11202, doi: 10.1029/2004JB003173.
[18] D. Patriarche, M.C. Castro, P. Goovaerts, Estimating regional hydraulic conductivity fields— a comparative study of geostatistical methods, Math. Geol. 37 (6) (2005) 587–613, doi: 10.1007/s11004-005-7308-5.
[19] M.C. Castro, M. Stute, P. Schlosser, Comparison of the ^{4}He ages and ^{14}C ages in simple aquifer systems: implications for groundwater flow and chronologies, Appl. Geochem. 15 (2000) 1137–1167.
[20] D.G. Bebout, V.J. Gavenda, A.R. Gregory, S.C. Claypool, J.H. Han, J.H. Seo, Geothermal resources, Wilcox Group, Texas Gulf Coast, Bur. of Econ. Geol., Univ. of Tex. at Austin, Austin, Tex., USA, Report ORO/4891-3, 1978, 82 pp.
[21] H.S. Hamlin, Depositional and ground-water flow systems of the Carrizo–Upper Wilcox, South Texas, Report of Investigations, vol. 175, Bur. of Econ. Geol., Austin, Tex., USA, 1988, 61 pp.
[22] H.B. Harris, Ground-water resources of La Salle and McMullen Counties, Texas, Bulletin, vol. 6520, Texas Water Commission, Austin, Tex., USA, 1965, 96 pp.
[23] W.H. Alexander Jr., D.E. White, Ground-water resources of Atascosa and Frio Counties, Texas, Report, vol. 32, Texas Water Development Board, Austin, Tex., USA, 1966, 211 pp.
[24] M.O. Saar, M.C. Castro, C.M. Hall, M. Manga, T.P. Rose, Quantifying magmatic, crustal, and atmospheric helium contributions to volcanic aquifers using all stable noble gases: implications for magmatism and groundwater flow, Geochem. Geophys. Geosyst. 6 (2005) Q03008, doi: 10.1029/2004GC000828.
[25] T. Torgersen, W.B. Clarke, Helium accumulation in groundwater, I: an evaluation of sources and the flux of crustal ^{4}He in the Great Artesian Basin, Geochim. Cosmochim. Acta 49 (5) (1985) 1211–1218.
[26] M.C. Castro, A. Jambon, G. de Marsily, P. Schlosser, Noble gases as natural tracers of water circulation in the Paris Basin 1. Measurements and discussion of their origin and mechanisms of vertical transport in the basin, Water Resour. Res. 34 (10) (1998) 2443–2466.
[27] M.C. Castro, P. Goblet, E. Ledoux, S. Violette, G. de Marsily, Noble gases as natural tracers of water circulation in the Paris Basin 2. Calibration of a groundwater flow model using noble gas isotope data, Water Resour. Res. 34 (10) (1998) 2467–2483.
[28] T.H.E. Heaton, J.C. Vogel, "Excess air" in groundwater, J. Hydrol. 50 (1–4) (1981) 201–216.
[29] C.J. Ballentine, C.M. Hall, Determining paleotemperature and other variables by using error-weighted, nonlinear inversion of noble gas concentrations in water, Geochim. Cosmochim. Acta 63 (16) (1999) 2315–2336.
[30] M.C. Castro, Helium sources in passive margin aquifers — new evidence for a significant mantle ^{3}He source in aquifers with unexpectedly low in-situ ^{3}He/^{4}He production, Earth Planet. Sci. Lett. 222 (3–4) (2004) 897–913, doi: 10.1016/j.epsl.2004.03.031.
[31] G. de Marsily, Quantitative Hydrogeology, Academic Press, San Diego, CA, USA, 1986 440 pp.
[32] D.J. Goode, Direct simulation of groundwater age, Water Resour. Res. 32 (2) (1996) 289–296.
[33] M. Varni, J. Carrera, Simulation of groundwater age distribution, Water Resour. Res. 12 (34) (1998) 3271–3281.
[34] E. Cordier, P. Goblet, Programme METIS- Simulation d'écoulement et de transport miscible en milieu poreux et fracturé, Centre d'Informatique Géologique, Ecole Nationale Supérieure des Mines de Paris, Fontainebleau, France, Notice d'emploi LHM/RD/99/18, 1999.
[35] C.E. Manning, S.E. Ingebritsen, Permeability of the continental crust; implications of geothermal data and metamorphic systems, Rev. Geophys. 37 (1) (1999) 127–150.
[36] W.B. Klemt, G.L. Duffin, G.R. Elder, Ground-water Resources of the Carrizo Aquifer in the Winter Garden Area of Texas, Report, vol. 210 (1), Texas Water Development Board, Austin, Tex., USA, 1976, 30 pp.
[37] LBG-Guyton Associates, HDR Engineering Inc., Interaction Between Ground Water and Surface Water in the Carrizo–Wilcox Aquifer, Texas Water Development Board, 1998 W600.8 C235.
[38] W. Aeschbach-Hertig, U. Beyerle, J. Holocher, F. Peeters, R. Kipfer, Excess air in groundwater as a potential indicator of past environmental changes, Study of Environmental Change using Isotope Techniques, IAEA, Vienna, 2002, pp. 174–183.
[39] Texas Water Development Board, Ground-Water Database, http://www.twdb.state.tx.us/publications/reports/GroundWaterReports/GWDatabaseReports/GWdatabaserpt.htm, 2003.
[40] K.H. Tan, Environmental Soil Science; Second Edition, Revised and Expanded, Marcel Dekker, New York, NY, USA, 2000 451 pp.
[41] S.A. Hall, Channel trenching and climatic-change in the Southern United-States Great-Plains, Geology 18 (4) (1990) 342–345.
[42] M.D. Blum, S. Valastro Jr., Response of the Pedernales River of central Texas to late Holocene climatic change, Ann. Assoc. Am. Geogr. 79 (3) (1989) 435–456.
[43] D.A. Hodell, J.H. Curtis, G.A. Jones, A. Higueragundy, M. Brenner, M.W. Binford, K.T. Dorsey, Reconstruction of Caribbean climate change over the past 10,500 years, Nature 352 (6338) (1991) 790–793.
[44] D.A. Hodell, M. Brenner, J.H. Curtis, T. Guilderson, Solar forcing of drought frequency in the Maya lowlands, Science 292 (5520) (2001) 1367–1370.

[45] R.B. Gill, The Great Mayan Droughts: Water, Life, and Death, University of New Mexico Press, Albuquerque, 2000 464 pp.
[46] G.B. Wilson, G.W. McNeill, Noble gas recharge temperatures and the excess air component, Appl. Geochem. 12 (6) (1997) 747–762.
[47] J.E. Brinkman, Water age dating of the Carrizo sand, Ph.D., Univ. of Arizona (1981) 131 pp.
[48] G.D. Smith, F. Newhall, L.H. Robinson, D. Swanson, Soil-temperature regimes — their characteristics and predictability, Technical Publication, vol. 144, U.S. Department of Agriculture Soil Conservation Service, 1964, 14 pp.
[49] N.M.J. Hall, P.J. Valdes, A GCM simulation of the climate 6000 years ago, J. Clim. 10 (1) (1997) 3–17.
[50] G. Vettoretti, W.R. Peltier, N.A. McFarlane, Simulations of mid-Holocene climate using an atmospheric general circulation model, J. Clim. 11 (10) (1998) 2607–2627.
[51] A. Kitoh, S. Murakami, H. Koide, A simulation of the Last Glacial Maximum with a coupled atmosphere–ocean GCM, Geophys. Res. Lett. 28 (11) (2001) 2221–2224.
[52] Z. Liu, S.P. Harrison, J. Kutzbach, B. Otto-Bliesner, Global monsoons in the mid-Holocene and oceanic feedback, Clim. Dyn. 22 (2–3) (2004) 157–182, doi: 10.1007/s00382-003-0372-y.